available at www.sciencedirect.com

ScienceDirect

journal homepage: www.elsevier.com/locate/ijrefrig

Design of a steady-state detector for fault detection and diagnosis of a residential air conditioner

Minsung Kim[a], *Seok Ho Yoon*[b], *Piotr A. Domanski*[b], *W. Vance Payne*[b,*]

[a]*Geothermal Energy Research Center, Korea Institute of Energy Research, Daejeon 305-343, Korea*
[b]*HVAC&R Equipment Performance Group, National Institute of Standards and Technology, 100 Bureau Drive, MS 8631, Gaithersburg, MD 20899, USA*

ARTICLE INFO

Article history:
Received 8 May 2007
Received in revised form
19 September 2007
Accepted 17 November 2007
Published online 28 November 2007

Keywords:
Air conditioner
Residential building
Compression system
Process
Detection
Fault
Steady state

ABSTRACT

This paper presents a general methodology for developing a steady-state detector for a vapor compression system based on a moving window and using standard deviations of seven measurements selected as features. The feature thresholds and optimized moving window size were based upon steady-state no-fault tests and startup transient tests. The study showed that evaporator superheat and condenser subcooling were sufficient for determining the onset of steady-state during the startup transient. However, they misidentified steady-state during indoor temperature change tests where evaporator saturation temperature and air temperature change across the evaporator were needed for proper steady-state identification. Hence, the paper recommends including all fault detection and diagnosis (FDD) features in the steady-state detector to ensure the robustness of the detector because different features may play key roles with different transients.

Published by Elsevier Ltd.

Conception d'un détecteur d'anomalie / outil diagnostique en régime stable pour un conditionneur d'air résidentiel

Mots clés : Conditionneur d'air ; Immeuble d'habitation ; Système à compression ; Procédé ; Détection ; Anomalie ; Régime stable

1. Introduction

Fault detection and diagnostic (FDD) methodologies can be developed to function during steady-state or transient operation of a system. Some of the transient fault analyses have been applied to whole building HVAC systems (Cho et al., 2005), to chiller refrigerant leak detection (Navarro-Esbri et al., 2007), and to compressor motor and other electrical faults (Armstrong et al., 2004). The original FDD publications and the majority of the research, however, have been

* *Corresponding author*. Tel.: +1 301 975 6663; fax: +1 301 975 8973.
E-mail address: vance.payne@nist.gov (W. Vance Payne).
0140-7007/$ – see front matter Published by Elsevier Ltd.
doi:10.1016/j.ijrefrig.2007.11.008

Nomenclature

Q	capacity
t	time
T	temperature (°C)
v	variance
x	measured data
$\bar{x}$	moving window average of measured data

Greek symbols

Δ	difference
σ	standard deviation about the mean value

Abbreviations and subscripts

A	air side
C	condenser
CA	air across the condenser
D	compressor discharge
E	evaporator
EA	air across the evaporator
FDD	fault detection and diagnosis
HVAC	heating, ventilating and air conditioning
i	feature index
ID	indoor or indoor dry-bulb temperature
IDP	indoor dew point temperature
k	index of time instant
MW	moving window
n	number of data samples in a moving window
OD	outdoor
RH	relative humidity
sc	subcooling
sh	superheat
ss	steady-state
TXV	thermostatic expansion valve

presented on steady-state FDD methodologies (e.g., Grimmelius et al., 1995; Stylianou and Nikanpour, 1996; Rossi et al., 1997; Navarro-Esbri et al., 2007; Glass et al., 1995; Rossi, 1995; Breuker and Braun, 1998; Li, 2004), which require a method for steady-state identification. Since the primary goal of these investigations was fault detection, they did not evaluate steady-state detectors in detail.

Some of the first investigations of system steady-state identification came from process control field studies (Mahuli et al., 1992; Cao and Rhinehart, 1995; Jiang et al., 2003). Steady-state can be detected by observing global system characteristics, e.g., capacity, or – more simply – by monitoring selected parameters. If the only goal was to check system performance, providing enough time to reach steady capacity and power input could be a sufficient approach. However, reaching steady capacity does not guarantee the actual steady-state of all parameters used in a particular FDD scheme, hence, identification of steady-state is an important task for a satisfactory FDD analysis.

The term ''steady-state'' is a misnomer in a rigorous sense because no system parameter is ever steady, and its readings will vary to some degree with time. Hence, identification of steady-state requires first establishing a definition of what steady-state is, and then evaluating whether the system in question satisfies this definition's criteria. To this goal, we will establish variability thresholds from mean values that selected parameters cannot exceed over a predefined time period, referred to as the time window, for steady-state to be declared. Hence, the thresholds represent the allowed variations, and we use them to gauge the observed variations of the selected features from their mean value. The time window is moving with time because the observations made in the past outside of our observation window no longer affect steady-state identification in the present.

2. Moving window for steady-state detection

The concept of the steady-state detector originates from noise filter theory. When a system is not steady, thermodynamic system parameters are highly unstable. The variance or standard deviation of important parameters is typically utilized to indicate the statistical spread within the data distribution and can be used to characterize random variation of the measured signals.

The most common and simple steady-state detectors analyze the data over a predefined moving window, as illustrated in Fig. 1. A predefined time interval is established over which important parameters are sampled at regular intervals. This produces an array of system parameters that are continuously updated and held in memory. Since a moving window replaces each data point within the timespan, the moving window average is equivalent to a low-pass filter. In this study, the moving window standard deviation is used to detect system steady-state.

The steady-state detector uses the calculation of the standard deviation of parameters in a recursive fashion. Suppose that at any instant k, the average of the latest n samples of a data sequence, x_i, is given by

$$\bar{x}_k = \frac{1}{n}\sum_{i=k-n+1}^{k} x_i \tag{1}$$

A difference between two averages of the latest n samples at the current time, k, and at the previous time instant, $k-1$, is

$$\bar{x}_k - \bar{x}_{k-1} = \frac{1}{n}\left[\sum_{i=k-n+1}^{k} x_i - \sum_{i=k-n}^{k-1} x_i\right] = \frac{1}{n}[x_k - x_{k-n}] \tag{2}$$

Rearranged, the current average is calculated by

$$\bar{x}_k = \bar{x}_{k-1} + \frac{1}{n}(x_k - x_{k-n}) \tag{3}$$

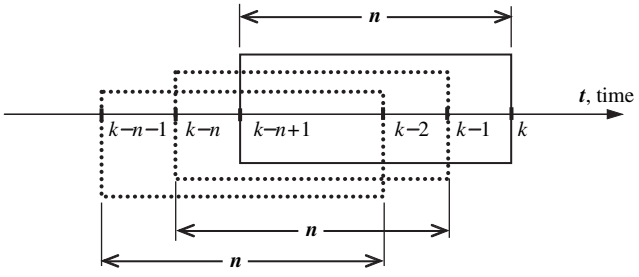

Fig. 1 – Moving windows of n data points at near k^{th} time.

This approach is known as a moving window average because the average at each kth instant is based on the most recent set of n values. In other words, at any instant, a moving window of n values is used to calculate the average of the next data sequence. A moving window variance can be defined similarly.

$$v_k = \frac{1}{n}\sum_{i=k-n+1}^{k}(x_i - \overline{x}_k)^2 = \frac{1}{n}\sum_{i=k-n+1}^{k} x_i^2 - \overline{x}_k^2 \quad (4)$$

$$v_k = v_{k-1} + \frac{1}{n}(x_k^2 - x_{k-n}^2) - (\overline{x}_k^2 - \overline{x}_{k-1}^2) \quad (5)$$

The moving window standard deviation is then given as

$$\sigma_k = \sqrt{v_k} \quad (6)$$

The steady-state detector identifies steady operation if the standard deviations for the selected features representing the status of the system fall below the defined threshold.

Li (2004) utilized moving window slopes and variances of evaporator exit superheat and liquid line subcooling as the key parameters of the steady-state detector in his FDD research on roof-top air conditioners. Glass et al. (1995) used geometrically weighted variance to identify a steady-state for air-handling units. Its main concept is that older data are exponentially attenuated by the multiplication of a "forgetting factor" based on the time constant during a system transition. The authors provided a recursive formulation for a digital application. Several FDD researches on vapor compression systems applied this method (e.g., Rossi, 1995; Breuker and Braun, 1998).

The moving window standard deviation can properly represent the state of the system when used with an optimized moving window size and feature thresholds. Since the moving window method has a fundamental structure, applying it to real systems imposes a small calculation load.

3. Development of the steady-state detector

3.1. *Laboratory setup and tests*

In this investigation, we used a split residential heat pump of 8.8 kW nominal cooling capacity and Seasonal Energy Efficiency Ratio (SEER; ARI Standard 210/240) of 13. The unit consisted of a compressor located with the outdoor coil, an indoor fan-coil section, cooling mode and heating mode thermostatic expansion valves (TXVs), and connecting tubing. Both the indoor and the outdoor coils were finned-tube type heat exchangers. We installed the unit in environmental chambers and charged with R410A according to the manufacturer's specifications. Fig. 2 illustrates the experimental setup. Additional specifications for the test rig, including indoor ductwork, indoor/outdoor unit dimensions, data acquisition and instrumentations, etc., were described in detail by Kim et al. (2006).

Our test included no-fault steady-state tests and no-fault startup transient tests for defining steady-state detection parameters. The startup transient tests were repeated three times to verify startup repeatability. Then we performed no-fault tests at indoor load change conditions to verify the performance of the developed detector. For the indoor load change tests, indoor dry-bulb temperature (T_{ID}) was varied by increasing or decreasing the number of energized electric air heaters within the indoor chamber supply duct. Table 1

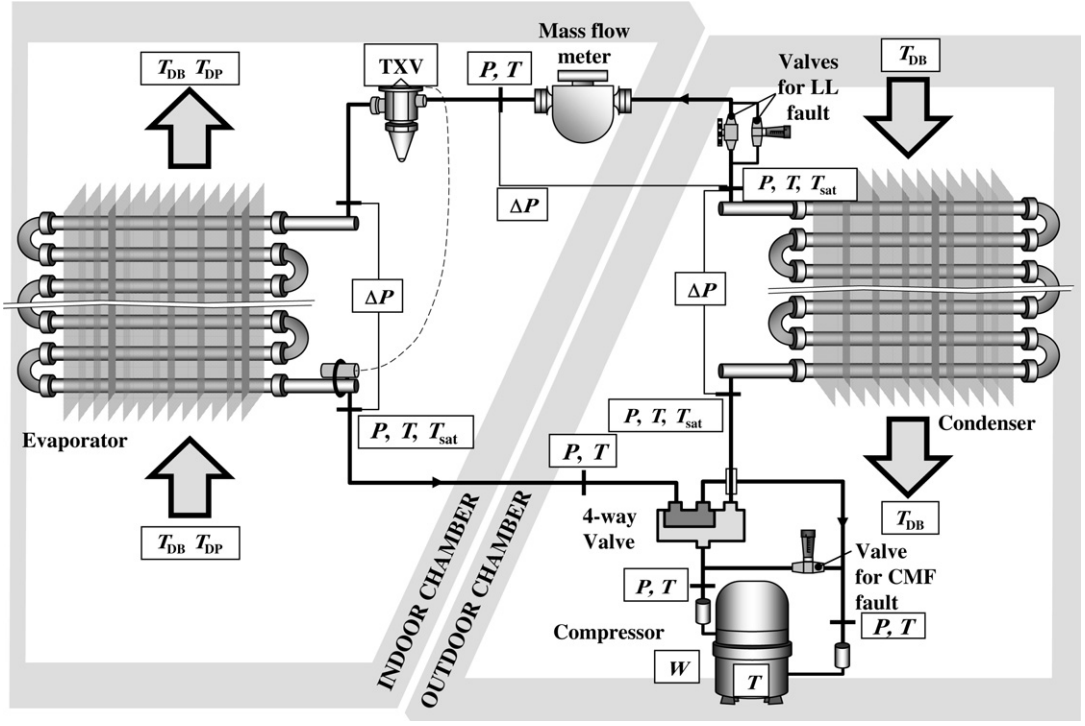

Fig. 2 – Schematic diagram of the experimental setup.

Table 1 – Types and conditions of no-fault tests

Test type	T_{OD} (°C)	T_{ID} (°C)	RH_{ID} (%)
Steady-state	27.8 ± 0.5	26.7 ± 0.5	50 ± 1.0
Startup transient	27.8 ± 0.5	26.7 ± 0.5	50 ± 1.0
Indoor load change	35.0 ± 0.5	15–35	20–80

shows the indoor and outdoor chamber conditions and standard deviations for these experiments.

3.2. *Measurement features*

We selected the following seven features: evaporator exit saturation temperature (T_E) and superheat (T_{sh}), condenser exit saturation temperature (T_C), compressor discharge temperature (T_D), liquid line subcooling (T_{sc}), air-side temperature drop across the evaporator (ΔT_{EA}), and air-side temperature gain across the condenser (ΔT_{CA}). In addition, we monitored the on–off status of the compressor. We used pressure transducers at the exits of the evaporator and the condenser to obtain T_E and T_C, respectively. The obtained pressures were converted into saturation temperatures using REFPROP 7 (Lemmon et al., 1998). For the other five features, T-type thermocouples were used.

3.3. *Setting feature thresholds based on steady-state data*

The threshold of each feature that bounds the mean steady-state signal is an important parameter in determining the performance of a steady-state detector. The smaller a threshold, the more conservatively steady-state is identified, and the more time it takes for the considered features to settle within their threshold ranges. Also, an excessively small threshold may cause the steady-state detector to never detect a steady-state especially under field conditions. Large thresholds, on the other hand, allow faster data collection but carry a risk of including some transient data and initiating false alarms. Therefore, the thresholds must be selected to both minimize the inclusion of non-steady-state data and maximize the recognition of steady-state.

To determine the steady-state detection thresholds for our heat pump/data collection hardware, we collected 47 data scans over 60 min after stable chamber conditions were achieved and the system stabilized. We accepted system stability criteria for steady-state tests as defined by ASHRAE Standard 37-2005; system's stability is attained after the equipment has operated for at least 1 h, and a four-sample moving window with sample rate of 10 min/sample yields a maximum range of 1.1 °C for indoor and outdoor air dry-bulb temperatures and a maximum range of 0.56 °C for wet-bulb temperatures. The mean value of the indoor and outdoor dry-bulb and wet-bulb temperatures for the four-sample moving window must not be greater than 0.28 °C and 0.17 °C, respectively, from the test condition setpoint.

We assumed a Gaussian distribution of the measured system parameters while the system was stable; therefore, a measurement of at least 30 data points was needed to assure a suitable estimate of the mean and standard deviation (Ott, 1984). We calculated the mean and standard deviations for all seven features, as listed in Table 2. Fig. 3 shows the variation and standard deviation of the steady-state data for T_{sh} and T_{sc}. We selected the value of $\pm 3\sigma$ as the steady-state threshold for selected features, i.e., we defined a feature as being in steady-state when its value falls within plus or minus three standard deviation, $\pm 3\sigma$, of its average value. Assuming that the steady-state measurements are random and normally distributed, the $\pm 3\sigma$ thresholds will filter out less than 1% of the steady-state data. Using the standard deviation thresholds of $\pm 1\sigma$ would lead to a very restrictive indication of steady-state.

In a physical sense, the calculated standard deviations of T_{sh} and T_{sc} represent the range of their "natural" fluctuation, which combine the effects of instability of the operating conditions induced by the environmental chambers, instability of the system itself, and instability of the data acquisition system. The standard deviations established from our steady-state tests should be considered the minimum standard deviations since they were attained at constant indoor and outdoor conditions as defined by the industry test standard and using dedicated, lab-quality instrumentation and data acquisition equipment. A manufacturer implementing this steady-state detector development technique must perform this exercise for their particular heat pump/data acquisition system combination to establish their standard deviations.

3.4. *Establishing the moving window size using startup transient tests*

Figs. 4–6, presented in this section, were derived from the same startup transient test. Fig. 4 displays variation of the seven features in the post-startup period. The figure demonstrates that T_{sh} and T_{sc} fluctuate the most and are the dominant indicators of system instability during startup. Fig. 5(a) further examines fluctuations of T_{sh} and T_{sc} showing them with $\pm 3\sigma$ thresholds superimposed (these thresholds were presented in Fig. 3). The vertical dashed line extending to Fig. 5(b) and (c) indicates the onset of steady-state at approximately 6 min and 30 s. From this point in time and on, the

Table 2 – Variations of selected features during steady-state

Features	T_{sh}	T_{sc}	T_E	T_D	T_C	ΔT_{CA}	ΔT_{EA}
Range[a] (°C)	0.49	0.22	0.14	0.25	0.17	0.27	0.25
Standard deviation, σ (°C)	0.124	0.052	0.024	0.058	0.035	0.063	0.058
Calculated thresholds, 3σ (°C)	0.37	0.16	0.07	0.17	0.11	0.19	0.17

a Difference between the maximum and the minimum value.

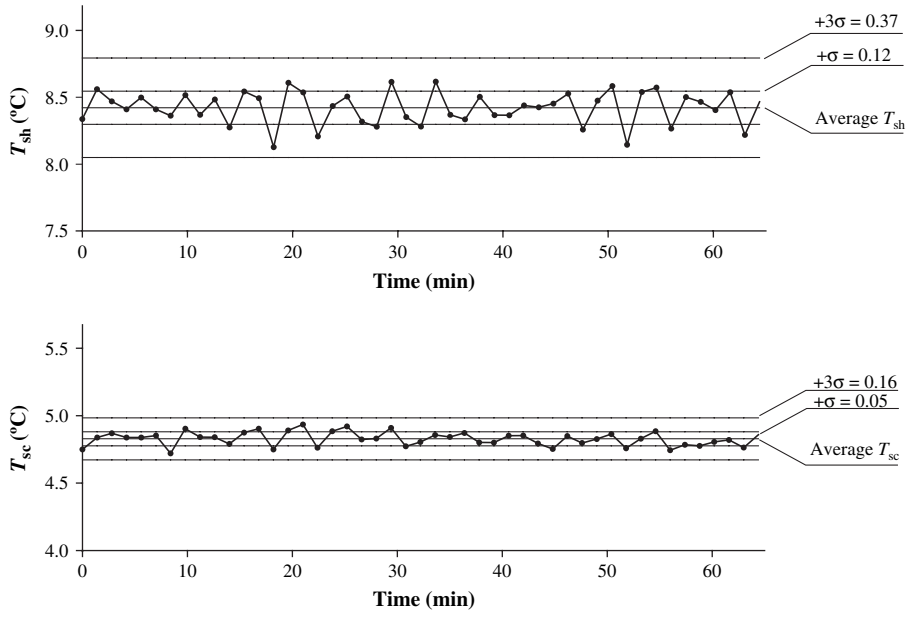

Fig. 3 – Variation of evaporator exit superheat and liquid line subcooling during steady-state operation, $T_{ID} = 26.7 \pm 0.5$ °C, $T_{OD} = 27.8 \pm 0.5$ °C.

values of both features are retained within their respective $\pm 3\sigma$ thresholds. While Fig. 5(a) convincingly shows us, based on individual measurements, that steady-state was attained at 6 min and 30 s after the startup, we must realize that we could make this determination only after extending the data collection much further in time beyond 6 min and 30 s to be able to calculate T_{sh} and T_{sc} mean values for steady-state operation. For this reason, using individual feature measurements for steady-state indication proves not to be a robust approach, and it is rather attractive to base a steady-state detector on some statistical quantity based upon measurements taken within a predefined moving time window. In this study we applied the $\pm 3\sigma$ steady-state thresholds and standard deviations of moving-window-measured T_{sh} and T_{sc} values, $\sigma_{MW}(T_{sh})$ and $\sigma_{MW}(T_{sc})$, for steady-state detection during the startup transient. Fig. 5(b) and (c) explains the procedure we used to determine the size of the moving window by showing T_{sh} and T_{sc} standard deviations, $\sigma_{MW}(T_{sh})$ and $\sigma_{MW}(T_{sc})$, respectively, for three windows sizes at a sample period of 14 s/sample: 70 s (MW70s), 140 s (MW140s), and 210 s (MW210s). It is our interest to establish the minimum window size for which the calculated $\sigma_{MW}(T_{sh})$ and $\sigma_{MW}(T_{sc})$ are below their respective threshold values past the onset of steady-state, which is shown in Fig. 5 to occur at 6 min and 30 s after startup.

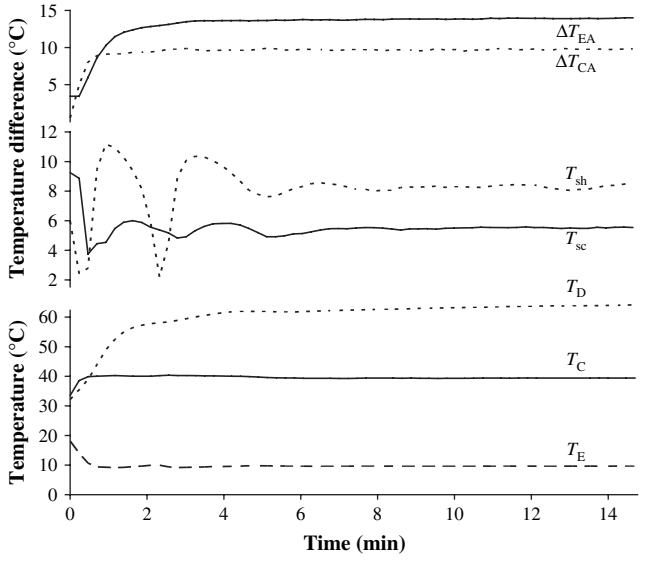

Fig. 4 – Variation of seven features during a startup transient, $T_{ID} = 26.7 \pm 0.5$ °C, $T_{OD} = 27.8 \pm 0.5$ °C.

The general procedure for determining the minimum moving window size, illustrated in Fig. 5, is as follows:

(1) Collect selected feature data during the startup period for at least 30 samples into the steady-state region at a sampling rate equal to the sampling rate used for steady-state sampling. The steady-state region is defined here to occur when the instantaneous values of the selected features fluctuate within $\pm 3\sigma$ of their steady-state mean values, as determined in Fig. 3. The dashed vertical line in Fig. 5(a) illustrates this onset of steady-state using the two most fluctuating FDD features during the startup, T_{sh} and T_{sc}.
(2) For all features, calculate the moving window standard deviation versus time for a range of moving window sample sizes, as presented in Fig. 5(b) and (c) for T_{sh} and T_{sc}.
(3) The moving window size that results in *all* features' standard deviations *crossing* and *remaining* within the $\pm 3\sigma$ threshold *after* steady-state is attained (as defined in Step 1), is the minimum acceptable moving window size.

The minimum acceptable moving window size (and thus sample size for our sampling rate) is determined by plotting the moving window standard deviations as a function of

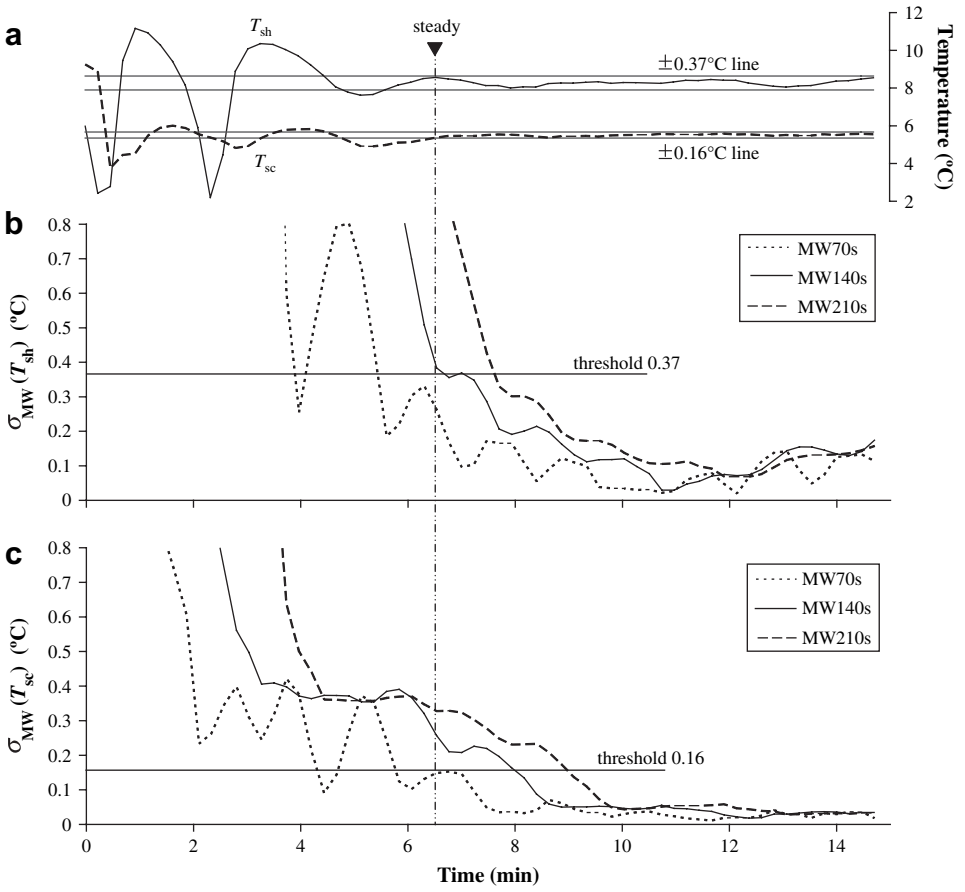

Fig. 5 – Onset of steady-state during a no-fault startup transient test, $T_{ID} = 26.7 \pm 0.5$ °C, $T_{OD} = 27.8 \pm 0.5$ °C. (a) Decision on steady-state, (b) $\sigma_{MW}(T_{sh})$ and (c) $\sigma_{MW}(T_{sc})$.

time for all features used in the FDD algorithm. In our case the last two features to vary within their $\pm 3\sigma$ thresholds, of all the features listed in Table 2, were T_{sc} and T_{sh}. The moving window standard deviations of T_{sh} and T_{sc} ($\sigma_{MW}(T_{sh})$ and $\sigma_{MW}(T_{sc})$) are plotted as a function of time in Fig. 5(b) and (c) with the vertical steady-state line determined in Fig. 5(a) extending down to indicate the onset time of steady-state.

Selecting the MW70s would not be appropriate because both $\sigma_{MW}(T_{sh})$ and $\sigma_{MW}(T_{sc})$ values calculated for this window

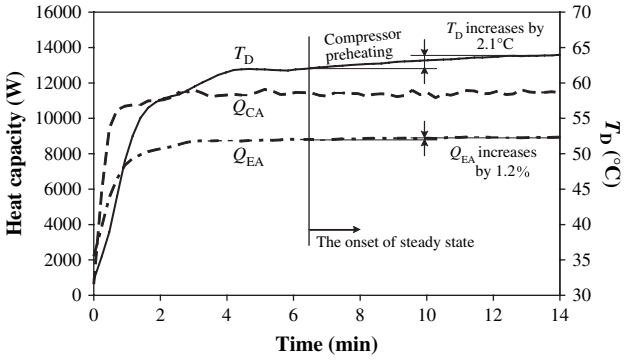

Fig. 6 – The startup transient of compressor discharge temperature and cooling and heating capacities, $T_{ID} = 26.7 \pm 0.5$ °C, $T_{OD} = 27.8 \pm 0.5$ °C.

size drop below the respective thresholds well before the onset of steady-state at 6 min and 30 s. The MW140s appears to be a good selection because it produces standard deviations that remain below the steady-state threshold after the vertical steady-state line; with a few seconds past this instance for $\sigma_{MW}(T_{sh})$ and 90 s later for $\sigma_{MW}(T_{sc})$ at 8 min. Hence, MW140s would indicate the onset of steady-state 90 s after it actually has occurred, but it would not provide a false indication of steady-state at any time earlier because of the relatively smooth and oscillation-free character of $\sigma_{MW}(T_{sh})$ and $\sigma_{MW}(T_{sc})$ lines. For MW210s, steady-state detection was indicated at approximately 9 min with $\sigma_{MW}(T_{sh})$ being the defining factor; this moving window could be acceptable, but it is not the minimum moving window size to satisfy our steady-state criteria that all features remain within their $\pm 3\sigma$ thresholds.

In this startup test, we took measurements every 14 s. We should note that the data sampling rate (samples/s or Hz) should be based upon a Nyquist frequency (greater than twice the frequency of the most varying feature) (Franklin et al., 1991), as determined by the frequency of variation in the features important to the FDD algorithm. For this investigation, the heat pump features during steady-state varied at a maximum frequency well below 0.03 Hz. Sampling at greater than twice this frequency, or one sample every 16 s, would capture all the feature variations. The sample rate fixed at one sample per 14 s was sufficient to eliminate or greatly reduce the

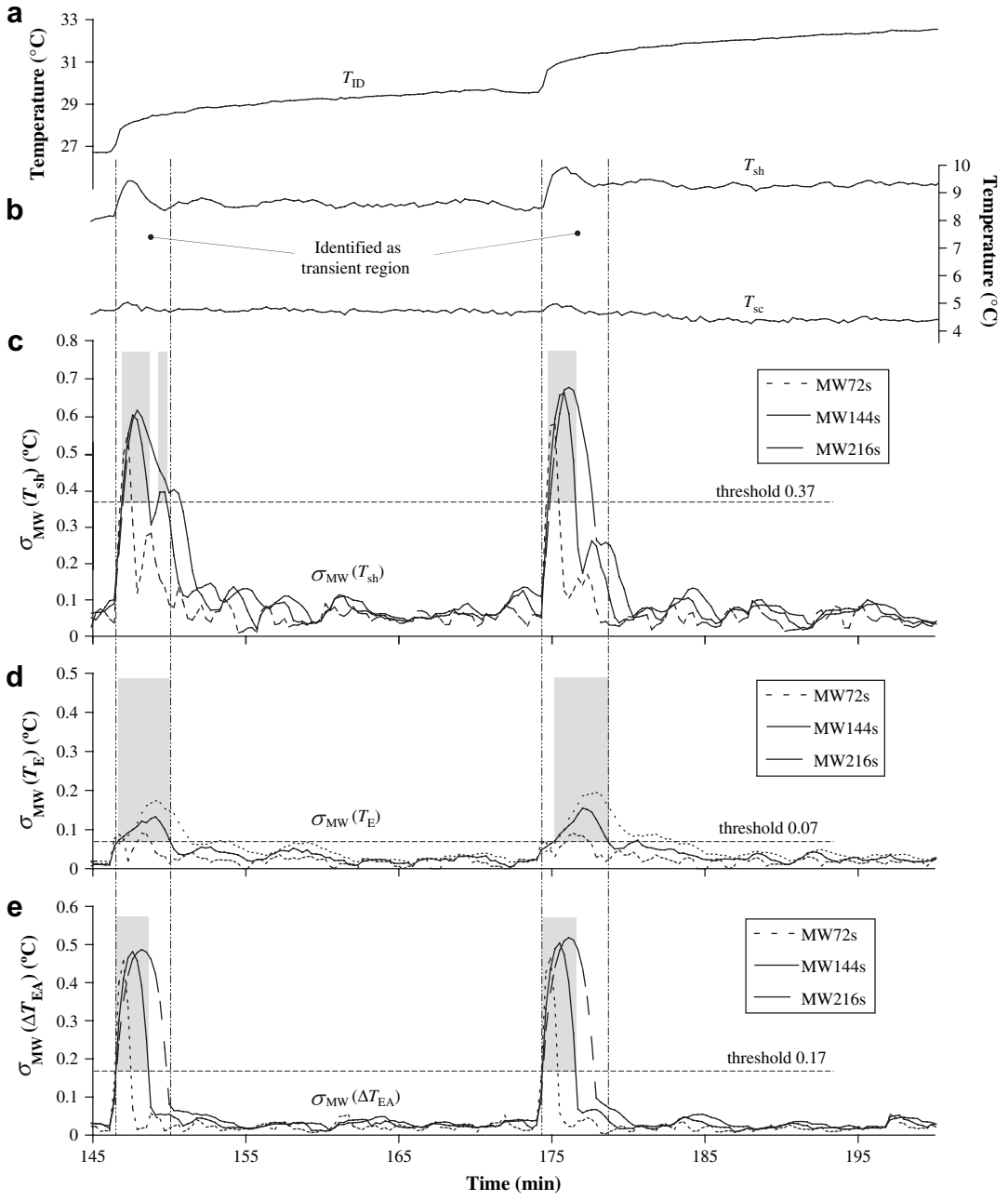

Fig. 7 – Identification of steady-state during a no-fault indoor load change test, $T_{OD} = 35 \pm 0.5$ °C. (a) T_{ID}, (b) T_{sh} and T_{sc}, (c) $\sigma_{MW}(T_{sh})$, (d) $\sigma_{MW}(T_E)$ and (e) $\sigma_{MW}(\Delta T_{EA})$.

likelihood of signal measurement bias. A greater sampling rate could be desirable, but sampling at much greater than the Nyquist frequency gains no new information.

As defined by the $\pm 3\sigma$ steady-state threshold, the system was stable approximately 6 min and 30 s after startup; however, the discharge line wall temperature, T_D, continued to increase. Fig. 6 shows that T_D increased by 2.1 °C for the remainder of the time shown in the figure while the evaporator capacity, Q_{EA}, increased by 1.3% with no change in the condenser capacity, Q_{CA}. The unchanging value of Q_{CA} tends to indicate a thermal inertia effect for T_D. The slow increase, or drift, in this temperature does not preclude its use as a fault detection feature, however, it will result in a higher uncertainty for T_D within the system's steady-state no-fault reference model.

4. Verification of the steady-state detector using an indoor load change test

4.1. *Test with no faults imposed*

Fig. 7 presents verification of the developed steady-state detection procedure during transients driven by changes in the indoor air temperature with no faults imposed. Stepped

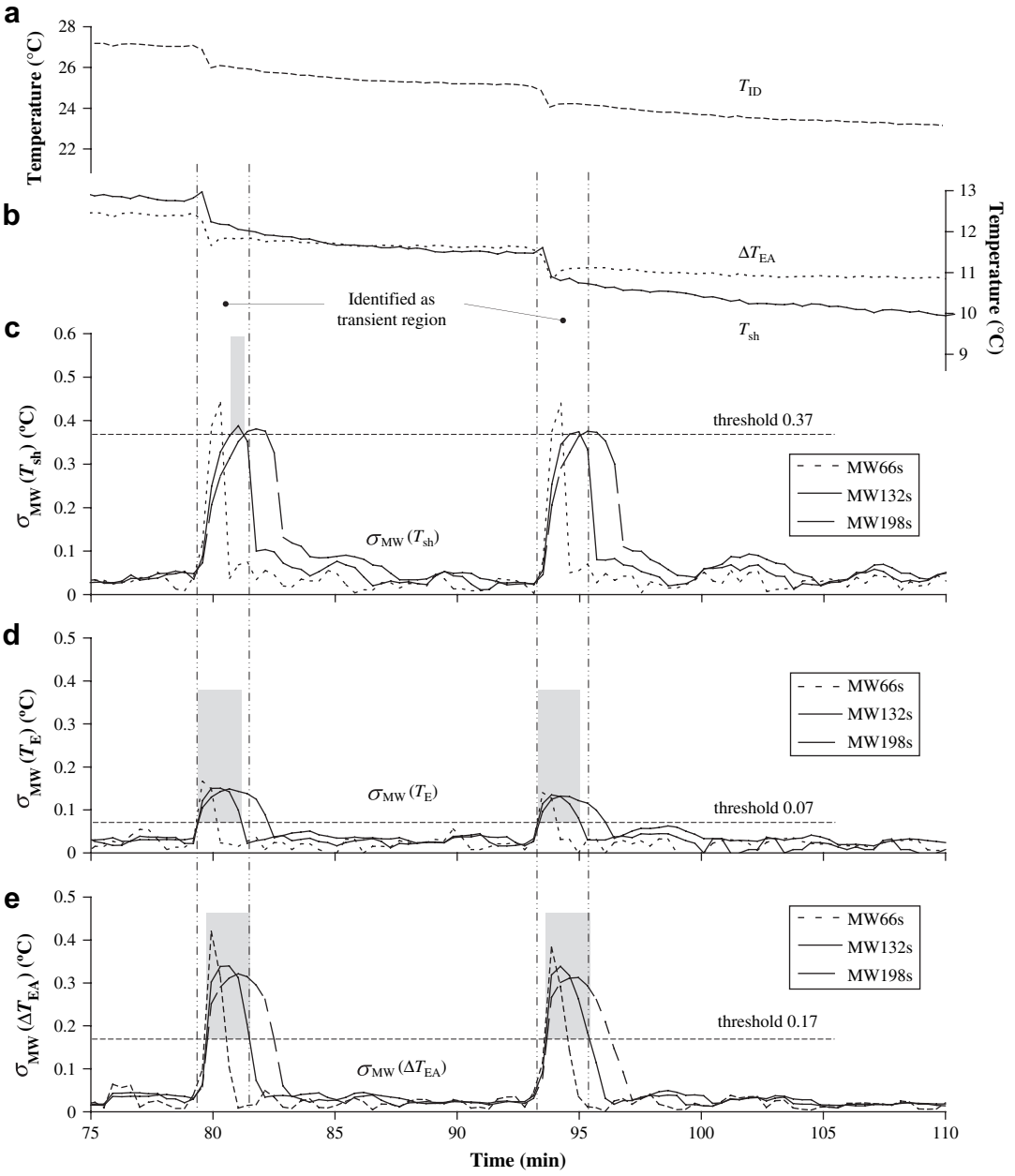

Fig. 8 – Identification of steady-state during an indoor load change test with a 20% refrigerant undercharge fault, $T_{OD} = 35 \pm 0.5$ °C. (a) T_{ID}, (b) T_{sh} and ΔT_{EA}, (c) $\sigma_{MW}(T_{sh})$, (d) $\sigma_{MW}(T_E)$ and (e) $\sigma_{MW}(\Delta T_{EA})$.

increases in T_{ID} in Fig. 7(a) reflect the energizing of additional indoor chamber electric duct heaters. In addition to T_{ID}, the figure shows T_{sh}, T_{sc}, and standard deviations of T_{sh}, T_E and ΔT_{EA} for an 18 s sample interval and moving window sizes of 72 s, 144 s, and 216 s. T_{sh}, T_{sc} and $\sigma_{MW}(T_{sh})$ are included because they were important during the startup transient. While T_{sh} shows some variation during an indoor load change test, T_{sc} is much more stable than during the startup transient.

The figures show two transient regions, which were identified using a 144 s moving window. The gray areas in the plots indicate transient regions for individual features as determined by the $\pm 3\sigma$ threshold steady-state detector algorithm within a 144 s moving window. Fig. 7(e) shows that ΔT_{EA} consistently indicates the beginning of the transient while Fig. 7(d) shows that T_E indicates the end of the transient. The variation of T_{sh} in Fig. 7(c) cannot filter out the whole transient region for all of these parameters. Instead, the variation of T_E and ΔT_{EA} in Fig. 7(d) and (e) controls the detection of steady-state. Since the transients in Fig. 7(a) are due to changes in T_{ID}, the features that characterize the evaporator (indoor coil), T_E and ΔT_{EA}, proved to be necessary for steady-state detection.

4.2. *Test with a 20% refrigerant undercharge fault*

Since the goal of an FDD scheme is to detect a system fault, the steady-state detector must be able to identify steady-state

during a system's faulty operation. For this reason, we applied the developed steady-state detector during a test with changing indoor temperature with a 20% refrigerant undercharge fault.

Fig. 8 shows the selected system parameters and features during the 35 °C outdoor temperature test. The moving window sizes are 66 s, 132 s, and 198 s with a data sampling rate of 22 s. Fig. 8(a) shows two rapid drops of T_{ID} due to turning off chamber electric duct heaters and a continuous decrease of T_{ID} due to chamber cooling by the tested system.

As during the fault-free indoor temperature change transient test, the change of $\sigma_{MW}(T_{sh})$ in Fig. 8(c) is not large enough to filter out the transient state, but changes in $\sigma_{MW}(T_E)$ and $\sigma_{MW}(\Delta T_{EA})$, taken together, correctly identify steady-state, as shown in Fig. 8(d) and (e). Hence, the same features identified steady-state during the undercharge fault and no-fault operations. Further, our review of transient data of the system operating under different faults indicated that the developed steady-state detector would work reliably with other faults as well.

5. Conclusions

We presented a methodology for developing a steady-state detector for a vapor compression system based on a moving window and using standard deviations of seven parameters selected as features. When the threshold band of the features was set at $\pm 3\sigma$ reflecting their fluctuations during steady-state operation, the optimal moving window size was approximately 140 s for a 14 s sampling rate. Of the seven monitored features, T_{sh} and T_{sc} measurements were sufficient for determining the onset of steady-state during the startup transient. However, they were not the dominant steady-state indicators during indoor temperature change tests, where T_E and ΔT_{EA} were needed for proper steady-state identification. Consequently, we recommend including all FDD features in the steady-state detector to ensure the robustness of the detector because different features may play key roles with different transients. While the proposed steady-state detector was developed from no-fault data, we verified that it can perform correctly with a faulty system.

A practical steady-state detector must be defined based upon the heat pump and system controller that will perform the fault detection and diagnosis. For any given system, the designer may choose FDD features other than those identified here. The system controller and instrumentation used in a commercial product most likely will have a different resolution or noise immunity than a dedicated lab-quality data acquisition system. This would translate into larger standard deviations and threshold values with different sampling rates and moving window sizes.

Acknowledgments

Minsung Kim's research at the National Institute of Standards and Technology, Gaithersburg, MD, was supported by a Korea Research Foundation Grant funded by the Korean Government (MOEHRD, Basic Research Promotion Fund No. M01-2003-000-20338-0).

REFERENCES

ARI Standard 210/240, 2006. Standard for Unitary Air-conditioning and Air-source Heat Pump Equipment. Air-Conditioning and Refrigeration Institute, 4100 North Fairfax Drive, Suite 200, Arlington, VA 22203.

ASHRAE Standard 37-2005, 2005. Methods of Testing for Rating Electrically Driven Unitary Air-conditioning and Heat Pump Equipment (ANSI Approved). American Society of Heating, Refrigerating and Air-Conditioning Engineers, 1791 Tullie Circle NE, Atlanta, GA 30329.

Armstrong, P., Norford, L., Leeb, S., July 2004. Fault detection in rooftop cooling equipment by power signature analysis. In: Proceeding of the 10th International Refrigeration Conference at Purdue University, West Lafayette, IN, USA.

Breuker, M.S., Braun, J.E., 1998. Evaluating the performance of a fault detection and diagnostic system for vapor compression equipment. HVAC&R Research 4 (4), 401–425.

Cao, S., Rhinehart, R., 1995. An efficient method for on-line identification of steady-state. Journal of Process Control 5 (6), 363–374.

Cho, S.H., Yang, H.C., Zaheer-uddin, M., Ahn, B.C., 2005. Transient pattern analysis for fault detection and diagnosis of HVAC systems. Energy Conversion and Management 46 (18–19), 3103–3116.

Franklin, G.F., Powell, J.D., Emami-Naeini, A., 1991. Feedback Control of Dynamic Systems, second ed. Addison-Wesley Publishing Company, Reading, MA USA, p. 617.

Glass, A.S., Gruber, P., Roos, M., Tödtli, J., 1995. Qualitative model-based fault detection in air-handling units. IEEE Control Systems Magazine 15 (4), 11–22.

Grimmelius, H.T., Woud, J.K., Been, G., 1995. On-line failure diagnosis for compression refrigeration plants. International Journal of Refrigeration 18 (1), 31–41.

Jiang, T., Chen, B., He, X., Stuart, P., 2003. Application of steady-state detection method based on wavelet transform. Computers and Chemical Engineering 27 (4), 569–578.

Kim, M., Payne, W.V., Domanski, P.A., Hermes, C.J.L., 2006. Performance of a Residential Heat Pump Operating in the Cooling Mode with Single Faults Imposed. National Institute of Standards and Technology, Nistir 7350, Gaithersburg, MD. http://www.bfrl.nist.gov/863/HVAC/pubs/index.htm

Li, H., 2004. A Decoupling-based Unified Fault Detection and Diagnosis approach for Packaged Air Conditioners. Ph.D. thesis, Purdue University, West Lafayette, IN.

Lemmon, E.W., McLinden, M.O., Huber, M.L., 1998. NIST Reference fluid thermodynamic and transport properties – REFPROP, Version 7.0. National Institute of Standards and Technology, Gaithersburg, MD USA.

Mahuli, S.K., Rhinehart, R., Riggs, J.B., 1992. Experimental demonstration of non-linear model-based in-line control of pH. Journal of Process Control 2 (3), 145–153.

Navarro-Esbri, J., Berbegall, V., Verdu, G., Cabello, R., Llopis, R., 2007. A low data requirement model of a variable-speed vapour compression refrigeration system based on neural networks. International Journal of Refrigeration, doi:10.1016/j.ijrefrig.2007.03.007.

Navarro-Esbri, J., Torrella, E., Cabello, R., 2007. A vapour compression chiller fault detection technique based on adaptive algorithms, application to on-line refrigerant leakage detection. International Journal of Refrigeration 29 (5), 716–723.

Ott, L., 1984. An Introduction to Statistical Methods in Data Analysis, second ed. Duxbury Press, Boston, MA USA, pp. 82–89.

Rossi, T.M., 1995. Detection, Diagnosis, and Evaluation of Faults in Vapor Compression Cycle Equipment. Ph.D. thesis, Purdue University, West Lafayette, IN.

Rossi, T.M., Braun, J.E., 1997. A statistical, rule-based fault detection and diagnostic method for vapor compression air conditioners. HVAC&R Research 3 (1), 19–37.

Stylianou, M., Nikanpour, D., 1996. Performance monitoring, fault detection, and diagnosis of reciprocating chillers. ASHRAE Transactions 102 (1), 615–627.